Applicability of the Klein-Gordon equation for pair production in vacuum and plasma

Haidar Al-Naseri [*] and Gert Brodin [†]

Department of Physics, Umeå University, SE-901 87 Umeå, Sweden

In this paper, a phase-space description of electron-positron pair creation will be applied, based on a Wigner transformation of the Klein-Gordon equation. The resulting theory is similar in many respects to the equations from the Dirac-Heisenberg-Wigner formalism. However, in the former case, all physics related to particle spin is neglected. In the present paper we compare the pair-production rate in vacuum and plasmas, with and without spin effects, in order to evaluate the accuracy and applicability of the spinless approximation. It is found that for modest frequencies of the electromagnetic field the pair production rate of the Klein-Gordon theory is a good approximation to the Dirac theory, provided the matter density is small enough for Pauli blocking to be neglected, and a factor of 2 related to the difference in the vacuum energy density is compensated for.

I. INTRODUCTION

The interest in strong field physics has increased in the past decades due to the rapid development of the laser facilities [1,2]. See, e.g., Refs. [3,4] for the recent developments in the research area. In the presence of a strong electromagnetic field, the vacuum can decay into electron-positron pairs. This process was first studied by Sauter in 1931 [5] and a rigorous mathematical description of this process was derived by Schwinger in 1951 [6]. Since then, the basic mechanism has been studied in a dynamical context and for more complicated field geometries. In particular, a study of the interplay between temporal and spatial variations of the fields has been done in Refs. [7–10]. To maximize the number of produced particles in the case of subcritical field strengths, a geometry of colliding laser pulses has been suggested in Refs. [11–14].

In spite of much progress in recent years [7–14], due to spin and chiral effects associated with Dirac fermions, various simplifying assumptions are typically needed when studying electron-positron pair production. A way to relax some of these assumptions concerning, e.g., the electromagnetic field geometry, is to study scalar QED, where the spin of the particles is ignored. Scalar QED models, based on the Klein-Gordon equation, are considerably less complicated than those derived from the Dirac equation. While it is known that many qualitative features regarding pair production are preserved when replacing fermionic QED with scalar QED [15–17], a better understanding of the differences and similarities is desirable, to know to what degree results from

scalar QED can be trusted. The purpose of the present paper is to study pair production in vacuum and plasmas, with and without including the particle spin properties, to highlight differences and similarities between the bosonic and fermionic results.

Various models and methods can be used when studying electron-positron pair production from vacuum and in plasmas.. This includes quantum kinetic theories, which can be applied for fermionic and bosonic pair production in electric fields [18]. Treatments, where a bosonic model of pair production has been used, are given in Refs. [19,20], and works on both bosonic and fermionic pair production in electric and magnetic fields can be found in Ref. [21]. Moreover, lattice quantum electrodynamics has been used to model scalar QED pair production [22].

In the present paper, we will use a phase-space approach, based on a gauge invariant Wigner transform of the evolution equations. In the fermionic case, this leads to the real-time Dirac-Heisenberg-Wigner (DHW) formalism, first derived in Ref. [23]. For the bosonic case, this corresponds to making a (gauge-invariant) Wigner transform of the Klein-Gordon equation, as was first derived in Ref. [24] with applications presented, e.g., in Refs. [24–29]. We will refer to these equations as the Klein-Gordon-Wigner (KGW) equations. We note that since both KGW and DHW are based on a phase-space approach, they are conceptually similar, and this facilitates a direct comparison of the results.

An important conclusion from our paper, which agrees with previous findings [6,30], is that KGW and DHW are in exact agreement for pair production in the zero frequency limit, provided a factor of 2 is compensated for. The factor of 2 is closely related to the difference between the fermionic and bosonic vacuum expectation values. When the frequency of the applied field is increased, the spin polarization current in the DHW formalism grows, which is associated with a gradually larger deviation between the bosonic and fermionic results. For significant pair production, the self-consistent field generated by the plasma currents becomes appreciable,

---

*haidar.al-naseri@umu.se
†gert.brodin@umu.se

and this tends to enhance the deviation between bosonic and fermionic dynamics. For even higher plasma densities, Pauli blocking can be important, which naturally cannot occur in the bosonic case.

The paper is organized as follows: In Sec. II we present the derivation of the KGW formalism. In Sec. III we derive the linear response of a plasma to electromagnetic waves. We make a comparison both to the classical dispersion relation (which is recovered in the appropriate limit) and to the results based on the DHW formalism. Next, numerical results for large fields (Schwinger) pair production are presented in Sec. IV. Here we compared the particle production in KGW and DHW using different scaling parameters. Finally, we present our conclusions in Sec. V.

II. KGW MODEL

In this section, we will make a brief derivation of the KGW formalism that has previously been derived by Ref. [24], which the reader may consult for more details. The starting point is the Klein-Gordon equation

$$[(\partial_\mu - ieA_\mu)(\partial_\mu + ieA_\mu) + m^2]\phi(\mathbf{r}, t) = 0 \qquad (1)$$

where e is the elementary charge, m is the mass of the electron, and $A^\mu = (A^0, \mathbf{A})$, where A^0 and $\mathbf{A}$ are the scalar and vector potential, respectively. This equation contains a second-order derivative in time. To transform the Klein-Gordon equation to phase space and obtain an explicit expression of the charge density in phase space, we express the Klein-Gordon equation in the representation of Feshbach and Villars [31]. In this representation, we have a first-order time derivative. The Klein-Gordon field is expressed by the two-component wave function

$$\Phi = \begin{pmatrix} \psi \\ \chi \end{pmatrix} \qquad (2)$$

where

$$\psi = \frac{1}{2}\left(\phi + \frac{i}{m}\frac{\partial\phi}{\partial t} - \frac{eA^0}{m}\right), \qquad (3)$$

$$\chi = \frac{1}{2}\left(\phi - \frac{i}{m}\frac{\partial\phi}{\partial t} + \frac{eA^0}{m}\right). \qquad (4)$$

In matrix representation we get

$$i\frac{\partial\Phi}{\partial t} = \left[\frac{1}{2m}\left(-i\frac{\partial}{\partial\mathbf{r}} - e\mathbf{A}\right)^2\begin{pmatrix} 1 & 1 \\ -1 & -1 \end{pmatrix}\right. $$
$$\left. + m\begin{pmatrix} 1 & 0 \\ 0 & -1 \end{pmatrix} + eA^0\mathbf{1}\right]\Phi \qquad (5)$$

where **1** is the identity matrix. This equation is first order in the time derivative and has a Schrödinger type of time evolution. The right-hand side of this equation can be interpreted as a Hamiltonian operator that will be used to find the time evolution in phase space. Next, we use the gauge-invariant

Wigner transformation

$$\hat{W}(\mathbf{r}, \mathbf{p}, t)$$
$$= \int d^3z \exp\left(i\mathbf{p}\cdot\mathbf{z} + ie\int_{-1/2}^{1/2} d\lambda\mathbf{z}\cdot\mathbf{A}(\mathbf{r}+\lambda\mathbf{z}, t)\right)\hat{C}(\mathbf{r}, t) \qquad (6)$$

where

$$\hat{C}(\mathbf{r}, t) = \{\Phi(\mathbf{r} + \mathbf{z}/2, t), \Phi(\mathbf{r} - \mathbf{z}/2, t)\}. \qquad (7)$$

The Wigner function is defined as the expectation value of the Wigner operator

$$W(\mathbf{r}, \mathbf{p}, t) = \langle\Omega|\hat{W}(\mathbf{r}, \mathbf{p}, t)|\Omega\rangle \qquad (8)$$

where $|\Omega\rangle\langle\Omega|$ is the state of the system in the Hilbert space. To find an evolution equation in phase space, we take the time derivative of Eq. (6) and use the Hamiltonian operator in Eq. (5). We use the Hartree approximation where the electromagnetic field is treated as a nonquantized field. Finally, we have an equation of motion of the Wigner function

$$iD_t W(\mathbf{r}, \mathbf{p}, t) = -\frac{i}{2}\hat{O}_1\{\sigma_3 + i\sigma_2, W\}$$
$$+ \hat{O}_2[\sigma_3 + i\sigma_2, W] + m[\sigma_1, W] \qquad (9)$$

where σ_i, with $i = 1, 2, 3$, are the Pauli matrices and

$$\hat{O}_1 = \frac{\mathbf{p}\cdot\nabla}{m} + \frac{\mathbf{p}}{m}\cdot e\int_{1/2}^{1/2} d\lambda\mathbf{B}(x + i\hbar\lambda\nabla_p) \times \nabla, \qquad (10)$$

$$\hat{O}_2 = \frac{\nabla^2}{4m} - \frac{p^2}{m} - \frac{e\hbar^2}{12m}\nabla\cdot(\mathbf{B}\times\nabla)$$
$$+ 2\frac{\mathbf{p}}{m}\cdot ie\hbar\int_{1/2}^{1/2} d\lambda\lambda\mathbf{B}(x + i\hbar\lambda\nabla_p) \times \nabla_p, \qquad (11)$$

$$D_t = \partial_t + e\int_{1/2}^{1/2} d\lambda\mathbf{E}(x + i\hbar\lambda\nabla_p)\cdot\nabla_p. \qquad (12)$$

For longer macroscopic scales, the nonlocal operators given by the integrals can be expanded in powers of $\hbar$. Thus, for example in the long-scale limit, we may use $D_t = \partial_t + e\mathbf{E}\cdot\nabla_p$, and similarly for the other operators [24]. The interpretation of the variables described by Eq. (9) is not simple. Thus we make an expansion of the Wigner function over the Pauli matrices σ_i and the identity matrix **1**:

$$W(\mathbf{r}, \mathbf{p}, t) = f_3(\mathbf{r}, \mathbf{p}, t)\mathbf{1} + \sum_{i=1}^{3} f_{3-i}(\mathbf{r}, \mathbf{p}, t)\sigma_i \qquad (13)$$

where the expansion coefficients f_i, with $i = 1$–3, will lead to four coupled partial differential equations (PDEs):

$$D_t f_0 = -\hat{O}_1(f_2 + f_3),$$
$$D_t f_1 = -\hat{O}_2(f_2 + f_3) + 2mf_2,$$
$$D_t f_2 = \hat{O}_2 f_1 + \hat{O}_1 f_0 - 2mf_1,$$
$$D_t f_3 = -\hat{O}_2 f_1 - \hat{O}_1 f_0. \qquad (14)$$

This PDE system is the final one that covers all physics of the Klein-Gordon equation. This system is closed by Maxwell's

equations with the sources

$$\rho = e \int d^3 p f_0, \tag{15}$$

$$\mathbf{J} = \frac{e}{m} \int d^3 \mathbf{p} \, \mathbf{p}(f_2 + f_3). \tag{16}$$

Compared to the DHW formalism [23] which is based on the Dirac equation, this system contains only four instead of 16 scalar equations. This makes the KGW formalism simpler to solve numerically. The four scalars of the KGW formalism have a straightforward physical interpretation, as can be seen from the following observables:

$$Q = e \int d^3 p \, d^3 x f_0, \tag{17}$$

$$\mathbf{J} = \frac{e}{m} \int d^3 p \, \mathbf{p}(f_2 + f_3), \tag{18}$$

$$W = \int d^3 p \, d^3 x \left[\frac{p^2}{2m}(f_2 + f_3) + m f_3 \right], \tag{19}$$

$$\mathbf{M} = \int d^3 p \, d^3 x \, \mathbf{p}(f_0 - f_1) \tag{20}$$

where Q is the total charge, $\mathbf{J}$ is the current density, W is the particle energy, and $\mathbf{M}$ is the momentum. Interpretations that can be done from the above expressions include, e.g., that $e f_0$ is the (phase-space) charge density and $e \mathbf{p}/m(f_2 + f_3)$ is the current density, as implied by the sources in Maxwell's equations.

The f_i functions have the vacuum contribution

$$f_0 = f_1 = 0,$$
$$f_2 + f_3 = \frac{m}{\epsilon},$$
$$f_3 - f_2 = \frac{\epsilon}{m} \tag{21}$$

where $\epsilon = \sqrt{m^2 + p^2}$. The expressions above are obtained by calculating the Wigner operator for the free particle Klein-Gordon equation and taking the vacuum expectation value. If we add a plasma to the background, we should modify the source terms for $f_2 + f_3$ and $f_3 - f_2$. Moreover, the charge density f_0 should be nonzero. Adding electron and positron sources we first obtain $f_2 + f_3 = (m/\epsilon)F$ and $f_3 - f_2 = (\epsilon/m)F$ in Eq. (21) where

$$F = 1 + 2f_e(\mathbf{p}) + 2f_p(\mathbf{p}). \tag{22}$$

Here $f_{e,p}$ can be viewed as classical electron and positron distribution functions. Note that we have a positive sign between the particle and vacuum sources, instead of a negative one as in the DHW formalism [23,32]. This is related to the physics of the Pauli-exclusion principle, which obviously is not included in the KGW formalism, as the model is derived for spinless particles. By contrast, in the DHW formalism, the Pauli principle will be respected provided the correct expectation values for the vacuum states are implemented. Moreover, we can note that the particle contributions to F have an extra factor of 2 in Eq. (22), as compared to DHW formalism. This is due to the fact that the magnitude of the vacuum contribution is only half as large for spinless particles.

More formally, the particle contribution in Eq. (22) can be determined by demanding that particles present in the initial conditions contribute by the proper amount to the charge density, current density, momentum density, etc. Naturally, the particle contribution from electrons and positrons will depend on the number density $n_{0e,p}$ (where the index e, p denotes the number density of electrons and positrons, respectively). Using the same normalization as for the DHW formalism [32], $n_{0,e,p} = [2/(2\pi\hbar)^3] \int f_{e,p} d^3 p$, the factor of 2 in Eq. (22) for the particle contribution to the charge density follows.

With one reservation (see the last paragraph of this section), the functions $f_{e/p}$ can be picked as any common background distribution function from standard kinetic theory, i.e., a Maxwell-Boltzmann, Synge-Juttner, or Fermi-Dirac distribution, depending on whether the characteristic kinetic energy is relativistic and whether the particles are degenerate. In conclusion, initial conditions for the KGW variables involving a homogeneous medium with electron and positron distribution functions $f_{e,p}$ are given by

$$f_0 = 2f_p - 2f_e,$$
$$f_1 = 0,$$
$$f_2 + f_3 = \frac{m}{\epsilon}F,$$
$$f_3 - f_2 = \frac{\epsilon}{m}F \tag{23}$$

with F given by Eq. (22). The above expression gives a time-independent solution to the KGW equations in the absence of electromagnetic fields (assuming that the total charge density and current density are zero). The expressions in Eq. (23), describing the equilibrium states, are a necessary prerequisite for including dynamical scenarios, leading to particle pair creation as will be studied in the next sections.

Before ending this section, we note that when studying background distributions of electrons or positrons containing particle beams, there is one key difference between distribution functions of the KGW (and DHW) type, and of classical distribution functions. In the nonclassical theories of DHW and KGW, electrons and positrons are described with the same phase-space variables, specifically f_0 and $f_2 + f_3$ will give the phase-space charge and current densities for both electrons and positrons. For symmetric distributions, where $f(\mathbf{p}) = f(-\mathbf{p})$, such as, e.g., for thermodynamic background distributions, this will not lead to confusion when translating a classical distribution function into its KGW and DHW counterparts. However, just as for the DHW theory [33], the fact that antiparticles can be viewed as particles moving backward in time means that similar classical electron and positron momentum distributions f_e and f_p fulfill a "momentum mirror property" and should be represented as $f_e(\mathbf{p}) = f_p(-\mathbf{p})$. For a time-independent homogeneous distribution where $f_1 = 0$, two identical distributions (classically speaking) of electrons and positrons with a nonzero net drift must have the phase-space charge density $f_0 = f_{0e} + f_{0p} = f_{0e}(\mathbf{p}) - f_{0e}(-\mathbf{p})$ such that (in case of identical classical distributions) the phase-space charge density is an odd function of momentum $f_0(-\mathbf{p}) = -f_0(\mathbf{p})$. This means that, although the charge density vanishes after momentum integration as required, the momentum density that is also proportional to an integral over f_0 [see Eq. (20) with $f_1 = 0$] will survive for a drifting system, as required. However, the same argument also

implies that $f_2(-\mathbf{p}) + f_3(-\mathbf{p}) = f_2(\mathbf{p}) + f_3(\mathbf{p})$, such that the current density integrates to zero [see Eq. (18)], as required for electron and positron beams moving together.

III. LINEAR WAVES

In this section, we consider the linear response of a plasma to an electromagnetic wave field, accounting also for the contribution from the vacuum expectation values. For our case with no background electromagnetic fields, as described in the previous section, we get the unperturbed vacuum contributions as the Wigner transform of the expectation value of the free Klein-Gordon field operators. Thus, Eq. (23) (including the plasma) applies for the background. For the wave perturbation, we consider electromagnetic waves with the following geometry:

$$\mathbf{E} = E\mathbf{e}_x,$$
$$\mathbf{k} = k\mathbf{e}_z,$$
$$\mathbf{B} = B\mathbf{e}_y. \tag{24}$$

The ions will not be treated dynamically but will constitute a constant neutralizing background. In the absence of ions, nat-urally, the electron and positron background charge densities must cancel for the background to be in equilibrium. However, in the presence of a constant (immobile) ion background, the electron and positron may differ; in particular, the positron background may vanish.

Next, in order to study linear theory, we divide the functions f_i as

$$f_i(z, \mathbf{p}, t) = f_i^0(\mathbf{p}) + f_i^1(\mathbf{p})e^{i(kz-\omega t)} \tag{25}$$

where the upper indices denote unperturbed and perturbed quantities. Furthermore, we use Ampère's law to obtain an implicit dispersion relation that can be written as

$$D(k, \omega) = \omega^2 - k^2 + i\omega J_x$$
$$= \omega^2 - k^2 + \frac{ie\omega}{(2\pi\hbar)^3 E}\int d^3p\frac{p_x}{m}(f_3^1 + f_2^1) = 0. \tag{26}$$

After some algebra, we can compute the current sources and deduce the explicit expression

$$D(k, \omega) = \omega^2 - k^2 + \frac{e^2}{(2\pi\hbar)^3}\int d^3p\frac{p_x}{\omega^2 - k^2 - 4\epsilon^2 + 4k^2p_z^2/\omega^2}\left\{[\omega^2 - 2(p + \hbar k/2)^2 - 4m^2]\right.$$

$$\times\left[\Delta_1\mathbf{\nabla}_{p_x} - \frac{2\hbar k}{\omega^2}\left(\frac{\hbar\mathbf{k}}{12} - 2\mathbf{p}\Delta_2\right)\cdot(\mathbf{e}_y\times\mathbf{\nabla}_p)\right]\left(\frac{2m^2 + p^2}{2m\epsilon}F - \frac{p^2}{2m\epsilon}F\right) - 2\Delta_1\mathbf{\nabla}_{p_x}\frac{p^2}{\epsilon}F + 8\frac{k}{\omega}p_x\Delta_1\mathbf{\nabla}_{p_z}(f_e - f_p)$$

$$\left. - 4\frac{k^2}{\omega^2}p_z(p_x\mathbf{\nabla}_{p_z} - p_z\mathbf{\nabla}_{p_x})\Delta_1\frac{F}{\epsilon} - 4[(p + \hbar k/2)^2 + 2m^2]\frac{\hbar k}{\omega^2}\left(\frac{\hbar\mathbf{k}}{12} - 2\mathbf{p}\Delta_2\right)\cdot(\mathbf{e}_y\times\mathbf{\nabla}_p)\frac{F}{\epsilon}\right\} = 0 \tag{27}$$

where

$$\Delta_1 = \int_{1/2}^{1/2}d\lambda\cos(\hbar k\lambda\mathbf{\nabla}_{pz}), \tag{28}$$

$$\Delta_2 = \int_{1/2}^{1/2}d\lambda\lambda\sin(\hbar k\lambda\mathbf{\nabla}_{pz}). \tag{29}$$

Here the operators are given by $\Delta_1 = 1$ and $\Delta_2 = \hbar k\mathbf{\nabla}_{pz}/12$ in the long-scale limit, where we have kept contributions to the lowest nonvanishing order. We can obtain the classical limit by letting $\hbar \longrightarrow 0$ in Eq. (27). Doing so, we get $\Delta_2 = 0$. The dispersion relation then reduces to

$$D(k, \omega) = \omega^2 - k^2 - \frac{e^2}{\hbar^3\pi^2}\int dp\,p^2\left[\left(1 - \frac{p^2}{3\epsilon^2}\right)\frac{f_e + f_p}{\epsilon}\right.$$
$$\left. - \frac{kp^2}{3\epsilon^2}\left(\frac{1}{\omega + kp_z/\epsilon} - \frac{1}{\omega - kp_z/\epsilon}\right)\frac{\partial(f_e + f_p)}{\partial p_z}\right]$$
$$= 0 \tag{30}$$

which can be shown to agree with the standard result based on the relativistic Vlasov equation, after some straightfor-ward algebra. Here, f_e and f_p behave as classical distribution functions, except for the mirror property of the momentum dependence (which only is important when there is a back-ground drift) discussed at the end of Sec. II. We note that the

appearance of $\hbar$ in the integration measure is just a matter of normalization, and not a sign of any remaining quantum features [33].

Now, we want to compare the dispersion relation Eq. (27) with the DHW formalism. To be able to do that, we take the homogeneous limit of Eq. (27) (since only the electrostatic limit resulting from $k \longrightarrow 0$ has been computed in the DHW case) and compare it with the corresponding result from the DHW formalism [32,34]. Letting $k \longrightarrow 0$ in Eq. (27), and including electrons only in the background plasma $f = f_e$, we get

$$\omega^2 = -\frac{4e^2}{\pi^2\hbar^3}\int dp\frac{p^2\epsilon}{\hbar^2\omega^2 - 4\epsilon^2}$$
$$\times\left[\left(1 - \frac{p^2}{3\epsilon^2} - \frac{\hbar^2\omega^2}{4\epsilon^2}\right)f - \frac{\hbar^2\omega^2p^2}{24\epsilon^4}\right]. \tag{31}$$

For the DHW formalism, we apply the $k \longrightarrow 0$ result of the electrostatic case (see Refs. [32,34]), and we obtain

$$\omega^2 = -\frac{4e^2}{\pi^2\hbar^3}\int dp\frac{p^2\epsilon}{\hbar^2\omega^2 - 4\epsilon^2}$$
$$\times\left(1 - \frac{p^2}{3\epsilon^2}\right)\left(f - \frac{\hbar^2\omega^2}{4\epsilon^2}\right). \tag{32}$$

We can clearly see that the results agree in the classical limit, and that the denominators coincide, i.e., the physics related to wave-particle interaction is similar. Both for the KGW and DHW, the real part of the wave frequency ω_r is given by the classical limit to a good approximation. The reason is that for $\hbar\omega \sim m$, the Fermi energy E_F will be much larger than unity. Thus, even if $\hbar\omega \sim m$ we will have $\hbar\omega \ll E_f$, which, in turn, implies a minor quantum contribution to Eqs. (31) and (32). Nevertheless, there are also some differences between Eqs. (31) and (32). To focus on the most important one, we now concentrate on the damping given by the imaginary part of the wave frequency ω_i, associated with the pole contribution of the momentum integral. Using the Plemelj formula

$$\frac{1}{u-a} = P\frac{1}{u-a} + i\pi\delta(u-a) \tag{33}$$

where P is the principal value, we obtain from the KGW expression Eq. (31)

$$\omega_i = -\frac{e^2 p_{\text{res}}^3}{6\hbar^4 \omega_r^4 \pi}[1 + 2f(p_{\text{res}})]. \tag{34}$$

For the DHW system, we instead obtain

$$\omega_i = -\frac{e^2 p_{\text{res}}}{12\pi\hbar^2\omega}\left(1 + \frac{2m^2}{\hbar^2\omega_r^2}\right)[1 - f(p_{\text{res}})]. \tag{35}$$

Here p_{res} is the resonant momentum, making the denominators in the integrands zero, i.e., $m^2 + p_{\text{res}}^2 = \hbar^2\omega^2/4$. While some features of the two damping rates agree, it can be noted that there are also significant differences. These differences can be better understood in light of certain numerical results presented in the next section. Thus we will wait to make a more detailed comparison of the damping rates.

IV. NUMERICAL RESULTS

A. Preliminaries

Before presenting the numerical results, we discuss the issue of renormalization. For large momentum where we can use the approximation $\epsilon \approx p$, it is straightforward to see that the integrand in Eq. (31) scales as $1/p$, and thus the integral has a logarithmic divergence. In principle, this needs to be dealt with, but in practice, for a numerical solution, this is almost automatically solved by a numerical cutoff in the momentum integration that acts as an effective regularization. Due to the slow growth of the logarithmic divergence, in the presence of a numerical momentum cutoff, simply ignoring the issue of renormalization does not result in a significant error. The technical aspects are the same as for the DHW case, which has been described in more detail in Refs. [34,35].

To be able to compare the results of the numerical solution of Eq. (14) with the ones from the DHW formalism in [35], we consider the homogeneous limit of Eq. (14):

$$D_t f_0 = 0,$$

$$D_t f_1 = \frac{p^2}{m}(f_2 + f_3) + 2mf_2,$$

$$D_t f_2 = -\left(\frac{p^2}{m} + 2m\right)f_1,$$

$$D_t f_3 = \frac{p^2}{m}f_1. \tag{36}$$

Apparently, in the homogeneous limit, f_0 decouples, and we only need to solve three equations. To simplify the numerical solution, we define new variables as deviations from the vacuum state, i.e.,

$$\tilde{f}_i = f_i - f_{i,\text{vac}} \tag{37}$$

where

$$f_{1,\text{vac}} = 0,$$

$$f_{2,\text{vac}} = \frac{1}{2m\epsilon}(m^2 - \epsilon^2),$$

$$f_{3,\text{vac}} = \frac{1}{2m\epsilon}(m^2 + \epsilon^2). \tag{38}$$

With this choice, we make sure that our basic variables become small for large momenta, such that a momentum cutoff is possible. By introducing $\tilde{f}_i$, we remove the vacuum contribution from the variables that we solve numerically. Obviously, this does not mean that vacuum physics is not included in our solution; we only do this to handle certain numerical technicalities. The PDE system is now

$$D_t\tilde{f}_1 = \frac{p^2}{m}(\tilde{f}_2 + \tilde{f}_3) + 2m\tilde{f}_2,$$

$$D_t\tilde{f}_2 = \frac{eEp_z}{2m\epsilon}\left(1 + \frac{m^2}{\epsilon^2}\right) - \left(\frac{p^2}{m} + 2m\right)\tilde{f}_1,$$

$$D_t\tilde{f}_3 = -\frac{eEp_z}{2m\epsilon}p^2 + \frac{p^2}{m}\tilde{f}_1. \tag{39}$$

For notational convenience, we omit the tilde for variables in what follows. In order to solve the system numerically, we need to make some further adaptions. The next step is to make the additional change of variable

$$f_1 = f_1,$$

$$f_+ = f_2 + f_3,$$

$$f_- = f_2 - f_3; \tag{40}$$

introduce the canonical momentum q given by

$$q = p + eA; \tag{41}$$

and use normalized variables: $t_n = \omega_{ce}t$, $q_n = q/m$, $p_{n\perp} = p_\perp/m$, $E_n = E/E_{\text{cr}}$, and $A_n = eA/m$, where ω_{ce} is the Compton frequency. The final system resulting from these changes, which will be solved numerically, is

$$\partial_{t_n}f_1 = \epsilon_n^2 f_+ + f_-,$$

$$\partial_{t_n}f_+ = \frac{(q_n - A_n)}{\epsilon_n^3}E_n - 2f_1,$$

$$\partial_{t_n}f_- = \frac{q_n - A_n}{\epsilon_n}E_n - 2\epsilon_n^2 f_1 \tag{42}$$

together with Ampère's law

$$\frac{\partial E_n}{\partial t_n} = -\eta\int d^2p_n(q_n - A_n)f_+ \tag{43}$$

where $\eta = \alpha/\pi$, where α is the fine-structure constant. Note that, for notational convenience, we omit the subscript n for variables in what follows. The system Eqs. (42) and (43) is solved numerically using a phase-corrected staggered

leapfrog method [36]. Typical parameters of the simulations are a time step of the order of $\Delta t \approx 0.001$, a parallel momentum step $\Delta q \approx 0.01$, and a perpendicular momentum step $\Delta p_\perp \approx 0.1$. In spite of the rather good resolution in parallel momentum, the q dependence of the produced data tends to look noisy in momentum space. This is due to the Zitterbewegung effect which produces increasingly short scales. Nevertheless, the dynamics of the larger scales are not sensitive to the small-scale momentum details, i.e., changing Δq does not affect the results presented in this paper.

To confirm that the numerical scheme produces sound results, we study the energy conservation law. An energy conservation law of the system Eqs. (42) and (43) can be written in the form

$$\frac{d}{dt}\left[\frac{E^2}{2} + \frac{\eta}{2}\int d^2p((\epsilon^2+1)f_+ - f_-)\right] = 0. \quad (44)$$

For the numerical resolutions used in the runs presented below, the total energy of the system is conserved within a relative error typically less than 10^{-4}.

B. Effects due to the vacuum background

Before solving Eqs. (42) and (43) for more complicated scenarios, we can check the validity of the numerical solution by considering constant electric fields $E = E_0$. The rate for creating a fermionic pair from vacuum dn_f/dt is well known [6,30]:

$$\frac{dn_f}{dt} = \frac{1}{4\pi^3}\left(\frac{eE}{\hbar}\right)^2 \exp\left(-\frac{\pi E_{\mathrm{cr}}}{E}\right). \quad (45)$$

By comparison, the rate for creating a bosonic pair as described by the KGW theory is $dn_b/dt = 0.5 dn_f/dt$. This is a direct consequence of the factors given in Eq. (22), where the relative contribution from the vacuum sources is half of the contribution seen in the DHW formalism.

To validate the numerics, we will solve Eq. (42) and the corresponding equations in the DHW formalism [32] for the case of constant electric fields E_0 and only vacuum initially. Since our goal is to check the validity of the numerics by comparing with theory without back-reaction effects, we also neglect back-reaction, i.e., we do not solve Eq. (43) self-consistently. Then, we calculate the number of produced particles n_k in the KGW formalism and n_D in the DHW formalism, with n_k given by

$$n_k = \frac{1}{(2\hbar\pi)^3}\int d^3p \frac{1}{2\epsilon}[(\epsilon+1)f_+ - f_-]. \quad (46)$$

In Fig. 1, we compare the numerical values of $n_{k/D}$ with $dn_{b/f}/dt$ for different values of E_0. As can be seen, the numerical values follow the analytical ones with good agreement.

Interestingly, nothing prevents us from making a toy model where we use spinless dynamics for the evolution equations, but increase the vacuum expectation values by a factor of 2 in the KGW model. Doing this, for constant fields n_k will get the same behavior as n_D and thus the slightly modified version of the KGW formalism gives the exact same results as the DHW formalism
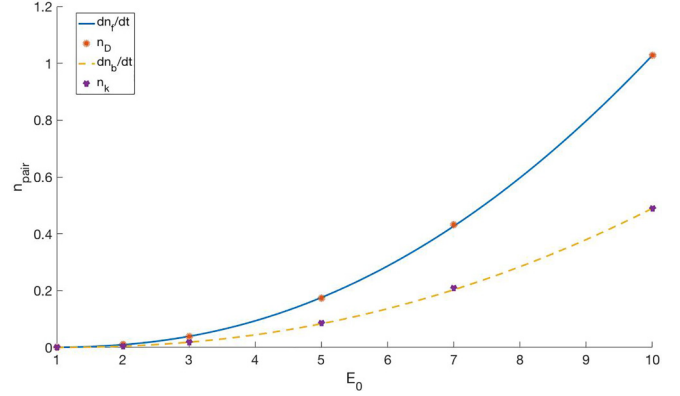

FIG. 1. The number of produced pairs from KGW (n_k) and DHW (n_D) using the numerical solutions together with the corresponding analytical results dn_b/dt and dn_f/dt.

C. High frequency effects

Now, we turn to the problem of time-dependent electric fields. We solve Eqs. (42) and (43) for the case with no plasma and only vacuum initially using the following representation of the time-dependent pulse:

$$E(t) = E_0 \mathrm{sech}\left(\frac{t}{b} - \tau_0\right)\sin\omega t \quad (47)$$

where τ_0 is the phase shift, b is the pulse length, and $\omega = N\omega_{ce}/100$. See Fig. 2 for a temporal plot of the electric pulse. We use n_k Eq. (46) to find the ratio n_k/n_D of the produced pair in KGW formalism and n_D in the DHW formalism [32]. For constant fields $E = E_0$, given by the rate presented for fermions in Eq. (45) and for bosons, we have

$$\frac{n_k}{n_D} = \frac{1}{2}. \quad (48)$$

For the case with a time-dependent electric field, in Fig. 3, we plot the ratio n_k/n_D versus ω. We can note that for small ω, i.e., in the constant field limit, the ratio is very close to 0.5 as expected. This is a good agreement between numerical and analytical solutions. For $\omega = 2$, we have $\hbar\omega = 2m$ and it is thus possible to create an electron-positron pair from a single quanta. For this case, the relative rate of the KGW
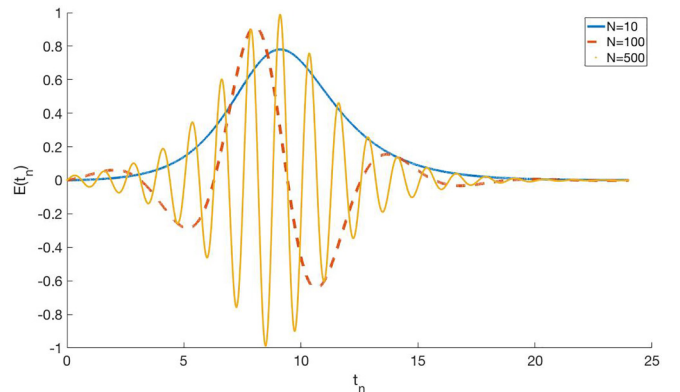

FIG. 2. The electric pulse is plotted over time for three different frequencies $N = (10, 100, 500)$.
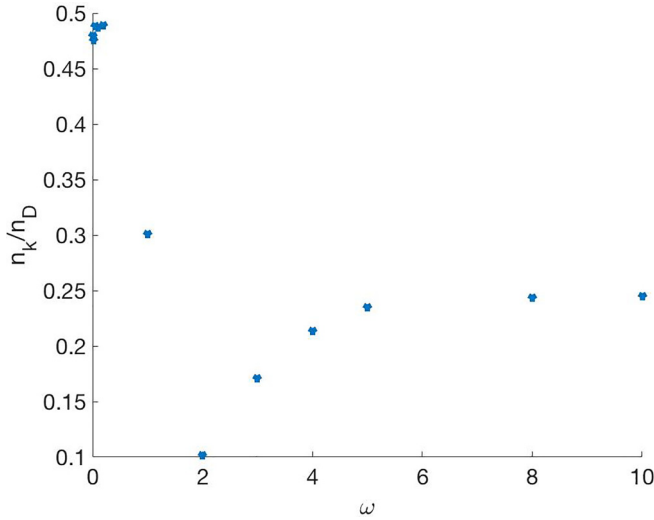
FIG. 3. The ratio n_k/n_D is plotted as a function of N, displaying the validity of the KGW formalism to model fermions at different regimes. Here we have used $E_0 = 1$.

pair production has a minimum. Generally, the ratio n_k/n_D tends to be smaller than 0.5 when processes involving few quanta (as opposed to the pure Schwinger mechanism) are possible to occur. This is because the probability of producing pairs from few quanta is smaller in the KGW description than in the DHW description. Looking specifically at one-quanta processes, this fact is confirmed in the linear damping results (where the linear damping is due to single quanta pair creation) as given by Eqs. (34) and (35). For frequencies $\hbar\omega \approx 2m_e$, we have p_{res} close to zero, and thus the created pairs have very small momentum. From Eq. (34), the damping of the wave in the KGW formalism scales as p_{res}^3, compared to the DHW formalism, where the wave damping is linear in p_{res}. For higher frequencies, we have larger p_{res} and this leads to a somewhat larger value of n_k/n_D, but it is still well below 0.5. The reason for the saturation of pair creation for

high frequencies in the KGW model is the scaling $\omega_i \sim \omega_r^{-4}$ in Eq. (34), more than compensating for the scaling $\omega_i \sim p_{res}^3$.

Since the KGW formalism is spinless, only free currents are created. By contrast, the total current in the DHW formalism is the sum of free current, the magnetization current [37], and the polarization current J_p [38]. Note, however, that in the absence of spatial variations, the magnetization current vanishes. For pulses with $\omega \ll \omega_{ce}$, the polarization current is small due to $J_p = \partial P/\partial t$, and the slow (compared to the Compton frequency) temporal scale. Here P is the polarization due to the particle spin properties. The smallness of the polarization current is confirmed in Fig. 4, where the polarization and total currents are plotted over time by solving the equations of the DHW formalism using the pulse in Eq. (47). For the upper panel of Fig. 4 where we used $N = 2$, i.e., $\omega = 0.02\omega_{ce}$, the polarization current is roughly only around 1% of the total current. When the frequency is increased to $N = 20$, the polarization current increases to about 10% of the total current. As the ratio $n_k/n_D = 1/2$ comes from the difference in the vacuum contribution only, the deviation from this value depends on the different dynamics of the KGW and DHW descriptions. For the present case, as long as the polarization current density J_p associated with the spin is small compared to the total current density, the dynamical influence of spin effects is comparatively small. Thus it is not surprising that the ratio $n_k/n_D = 1/2$ is relatively unaffected by the spin dynamics. However, a careful comparison of Figs. 3 and 4 shows that the deviation from $n_k/n_D = 1/2$ coincides with an increase in the relative importance of the spin dynamics.

Next, we would like to make contact between the analytical and numerical calculations. Specifically, we will study where in momentum space the pairs are produced. In Fig. 5, contour curves over the pair momentum density, i.e., the integrand in Eq. (46), are shown. The two figures in the upper panel show the contour for DHW expression $n_D(p_\perp, q)$ (the figure to the left) and the KGW expression $n_k(p_\perp, q)$ (the figure to the right) using the pulse in Eq. (47) with $\omega = 0.02\omega_{cr}$, $\tau_0 = \pi$, $b = 20$, and $E_0 = 1$. In the upper panel, we can see that
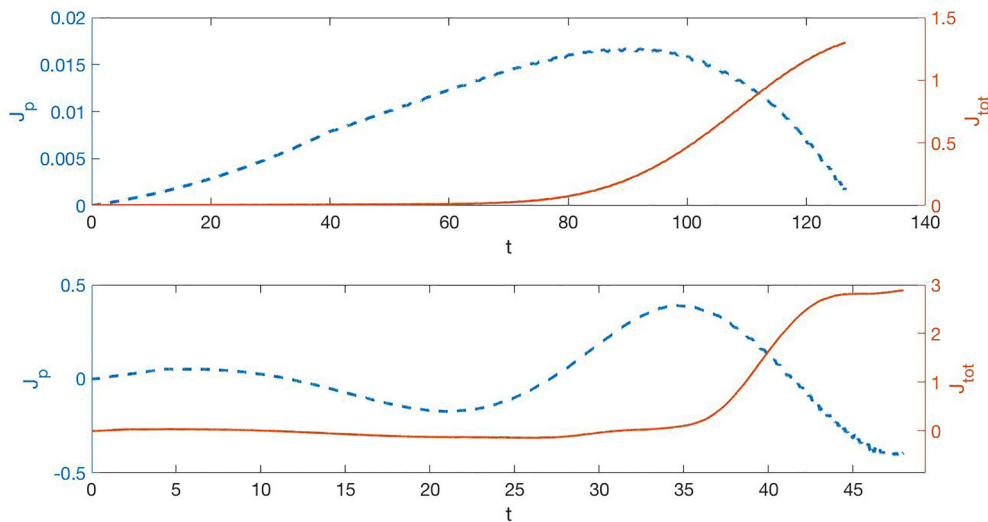

FIG. 4. Polarization current J_p and total current J_{tot} plotted over time for $N = (2, 20)$ in the upper and lower panels, respectively. Note the different scales for J_p and J_{tot}.
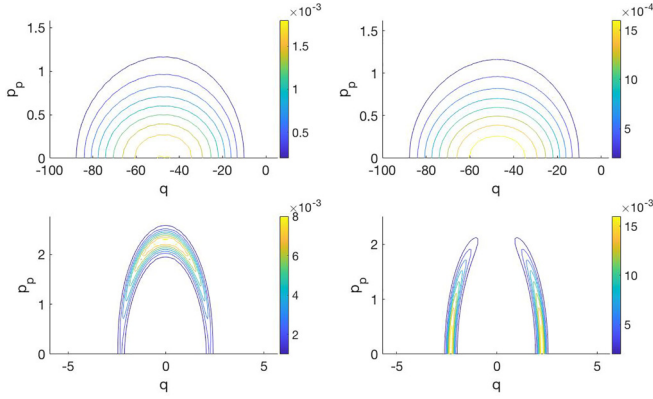
FIG. 5. Color mappings of the momentum distribution of the created pairs from DHW $n_D(q, p_\perp)$ (the first column) and KGW $n_k(q, p_\perp)$ (the second column). In the first panel, we have used $\omega = 0.02\omega_{ce}$, $\tau_0 = \pi$, $b = 20$, and $E_0 = 1$ and in the second panel we have used $\omega = 5\omega_{ce}$, $\tau_0 = \pi$, $b = 2$, and $E_0 = 2$.

created pairs have the same momentum distribution in both of the models. It should be emphasized that we here have used the toy model with the vacuum contribution twice as large as for a scalar field in the KGW calculations, to better mimic the behavior of fermions.

In the lower panel of Fig. 5, we have used the pulse in Eq. (47) with $\omega = 5\omega_{ce}$, $\tau_0 = \pi$, $b = 2$, and $E_0 = 2$. For such a high frequency, single quanta pair-creation processes dominate. Clearly, the polarization current J_p is important in this regime. As can be seen, in spite that pairs are created close to the region of resonant momenta, satisfying the resonance condition $m^2 + p_{res}^2 = \hbar^2\omega^2$, the different models have different momentum distributions nevertheless. For the KGW model (the figure to the right), the pairs created tend to have a higher value of $|q|$, and a smaller value of $p_\perp$. For the DHW model, the distribution in momentum space is the opposite.

To clarify the reason for this difference, we will rewrite the previous expressions Eqs. (31) and (32) in cylindrical momentum coordinates. In this case, the dispersion relation Eq. (31) for the KGW case becomes

$$\omega^2 = \frac{e^2}{4\pi^2\hbar^3} \int dp_\perp p_\perp dp_z \frac{1/\epsilon}{\hbar^2\omega^2 - 4\epsilon^2}$$
$$\times \left[2f(\hbar^2\omega^2 - 4\epsilon_\perp^2) + \hbar^2\omega^2 \frac{p_z^2}{\epsilon^2} \right] \qquad (49)$$

and the dispersion relation for the DHW case is written

$$\omega^2 = -\frac{e^2}{2\pi^2\hbar^3} \int dp_\perp p_\perp dp_z \frac{\epsilon_\perp^2/\epsilon}{\hbar^2\omega^2 - 4\epsilon^2}$$
$$\times \left(f - \frac{\hbar^2\omega^2}{4\epsilon^2} \right) \qquad (50)$$

where $\epsilon_\perp = \sqrt{m^2 + p_\perp^2}$. Note that we have regained p_z rather than q here [39] and also keep the un-normalized variables of Sec. III. The key to understanding the lower panels of Fig. 5 is the scalings with p_z and $p_\perp$ of the integrands in Eqs. (49) and (50). What contributes to the damping rates is the pair creation that results from the pole contribution. That is, pair creation

comes from an integration over resonant momenta p_{res}. The resulting pair creation will have a distribution in momentum space reflecting the magnitude of the integrand as a function of p_z and $p_\perp$ along the curve given by a constant p_{res}. As we are now considering pair creation in vacuum rather than a plasma, we can inspect the integrand in Eq. (49) with only the vacuum contribution present, in which case the integrand reads

$$\int dp_\perp p_\perp dp_z \frac{p_z^2/\epsilon^3}{\hbar^2\omega^2 - 4\epsilon^2}. \qquad (51)$$

Noting that the momentum which contributes to single-quanta pair creation will be close to the resonant momenta, we see that for resonant values with large p_z (q) and small $p_\perp$, we will get the dominant pair creation contribution. This is in agreement with the lower right panel of Fig. 5 as $p_\perp \approx 0$ gives a negligible pair creation rate.

For the left figure of the lower panel in Fig. 5, we have the contour curves of the momentum distribution for the created pairs in the DHW formalism. As noted above, we see that the created pairs tend to have a high perpendicular momentum. This effect has been seen in previous works [32,40]. Moreover, it is further confirmed by considering only the vacuum contribution to the integrand in Eq. (50):

$$\int dp_\perp p_\perp dp_z \frac{\epsilon_\perp^2/\epsilon^3}{\hbar^2\omega^2 - 4\epsilon^2}. \qquad (52)$$

We note that for resonant momenta, the integrand is largest for high perpendicular momentum and has a smaller value when $|p_z|$ is large, explaining why the momentum distribution of the single-quanta pair creation in the DHW formalism has the momentum distribution that we see in Fig. 5.

Next, we will include the effects due to back-reaction, i.e., we will solve Eq. (43) together with Eq. (42) using the pulse in Eq. (47). We start from vacuum and divide the electric field into the self-consistent electric field, given by the current sources generated by the created pairs, and the external electric field which is prescribed and given by the same type of temporal profile as before.

In Fig. 6, we have a plot of the self-consistent electric field (as the prescribed part is the same) over time comparing the results from DHW and KGW. In the first panel, we have used $N = 2$, i.e., $\omega = 0.02\omega_{ce}$. For this low frequency, we see a very good agreement between DHW and KGW. The good agreement is dependent on the choice to double the background vacuum contribution in the KGW model, i.e., we have imitated initial conditions for the fermions, even though the dynamical evolution follows that of a scalar field, neglecting the spin.

In the second panel, we use a slightly higher frequency $N = 4$. While the agreement is still good, we see a gradually growing phase shift between the DHW and KGW models. While the fraction n_K/n_D was almost unchanged when the frequency was increased to this value, when the self-consistent dynamic is involved, we see a higher sensitivity to the frequency. Increasing the frequency even higher to $0.1\omega_{ce}$, the difference between DHW and KGW is even more pronounced. Here, we see a more dramatic phase shift at an early stage and a qualitatively different evolution of the wave amplitude. Thus, modeling electron-positron pair creation with
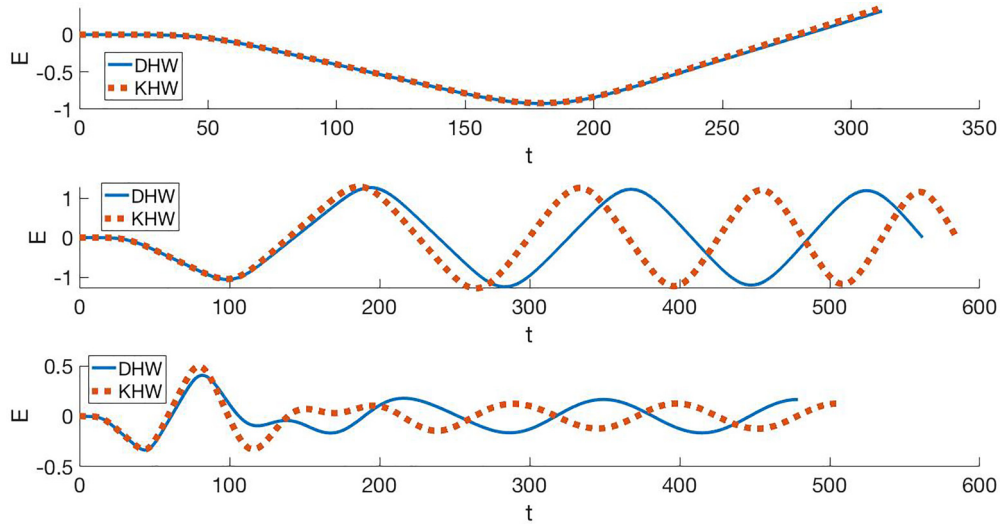
FIG. 6. The time profile of the self-consistent electric field from the KGW and DHW formalism for three values of the frequency of the initial electric pulse $\omega = (0.02, 0.04, 0.1)\omega_{ce}$, using the initial pulse with $E_0 = 1$, $b = 20$, and $\tau = \pi$.

the KGW model requires lower frequencies in the case of self-consistent dynamics.

The validity condition found here for the KGW theory, $\omega \leqslant 0.04$, is just a crude estimate, naturally. To a certain degree, it may also depend on the electric field magnitude. To illustrate this, let us compare the evolution for the KGW and DHW theory, using the same parameters as in panel 3 of Fig. 6, but with the external electric field amplitude increased from $E_0 = 1$ to 4. The temporal dependence of the electric field for the two cases is shown in Fig. 7. While certain qualitative features are the same, mainly plasma oscillations set up in the electron-positron plasma produced by the external field, there are also several distinct differences between the KGW and DHW case. First, the amplitude of the self-consistent field in the plasma oscillations is stronger for the DHW case. Second,

the plasma frequency is significantly higher in the KGW case, related to a higher amount of particles and a lower spread in the momentum distribution. Third, the damping of the plasma oscillations, resulting from further pair production due to the self-consistent electric field, is much more pronounced in the KGW case.

All in all, the differences between the KGW and the DHW case tend to increase with amplitude. This is due to two mechanisms. First, when the electric field is strong enough, a sufficient number of particles will be generated such that the Pauli blocking mechanism of fermions becomes significant. That an unlimited amount of particles can be generated in a limited region of momentum space for bosons is the reason why the plasma frequency is higher and the damping is stronger in the KGW case. Moreover, when more particles are generated due to a higher amplitude, the previous validity condition of a low enough frequency tends to be challenged simply due to a high (relatively speaking) plasma frequency. It can be seen in Fig. 7 that the frequency scale ω_p of the plasma oscillations is $\omega_p \approx 0.1$ for the KGW case, which is not within the validity regime of the frequency scale, but slightly higher.

D. Nondegeneracy effects

In this subsection, we would like to illustrate the mechanism of Pauli blocking. This mechanism is always present in the DHW formalism, but not in the KGW formalism as the model is spinless. However, whether or not Pauli blocking is an important feature dynamically depends on the number of free states where pairs can be created. In particular, a degenerate initial distribution will block the low-energy states in momentum space, which is the region where particles are most easily created. Thus, in this subsection, we will start with a plasma initially and solve Eqs. (42) and (43) and the corresponding equations in the DHW formalism. As initial conditions in the runs, we let $E(t = 0) = E_0$ and $A(t = 0) = 0$. The initial plasma is represented by a Fermi-Dirac
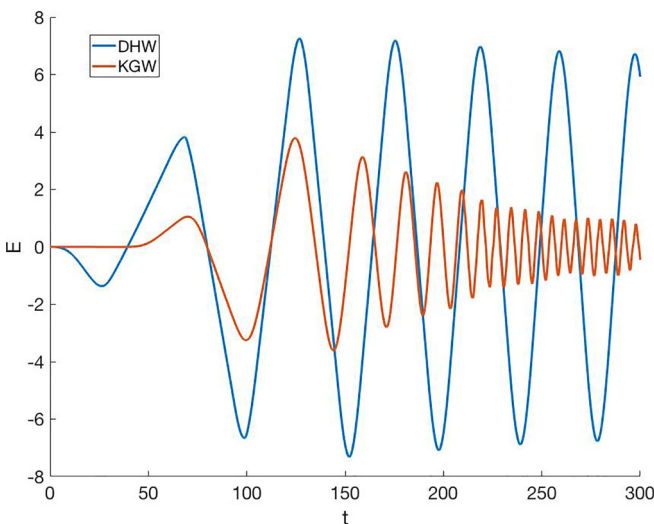

FIG. 7. The time profile of the self-consistent electric field from the KGW and DHW formalism using the initial pulse with $E_0 = 4$, $b = 20$, $\omega = 0.1\omega_{ce}$, and $\tau = \pi$.
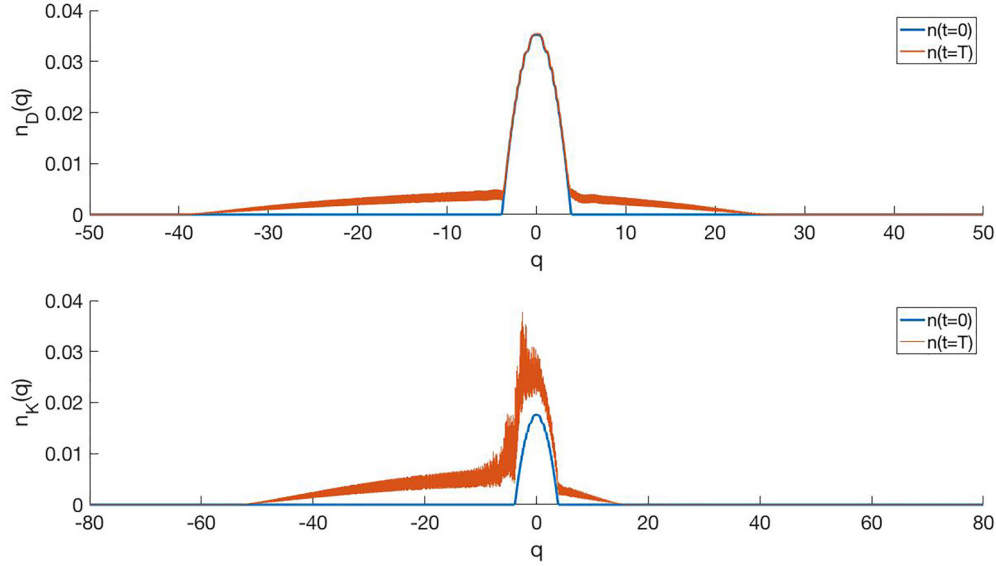
FIG. 8. The number density $n_{D/K}(q) = \int dp_\perp p_\perp n_{D/K}(q, p_\perp)$ as a function of the canonical momentum is plotted for $E_0 = 4$, $\mu = 4$, and $T = 0.02$ for DHW and KGW. Here, the solid curve is for $n\,(t = 0)$ and the thicker curve is for $n\,(t = T_p)$.

distribution:

$$f(q, p_\perp) = \frac{1}{1 + \exp{(\epsilon - \mu)/T}} \qquad (53)$$

where μ is the chemical potential and T is the temperature (we normalize both μ and T with the electron mass). For $\mu \gg T$, the chemical potential fulfills $\mu \approx E_F$, where E_F is the Fermi energy, in which case the distribution will be degenerate (i.e., we will have $f \approx 1$, i.e., all electron states filled, for energies smaller than the Fermi energy, and $f \approx 0$ otherwise). Naturally, nondegenerate initial distributions are still possible when using Eq. (53), by letting $\mu < T$. Also, by picking a large but negative chemical potential, we get a Maxwell-Boltzmann type of distribution. In principle, one could also study the case of an initial Bose-Einstein distribution, since the system can be solved for arbitrary initial conditions. However, since our aim is to see to what degree the KGW model can be applied for electrons and positrons, rather than actual bosons, we will not pursue that here.

In Fig. 8, we demonstrate the Pauli blocking mechanism. In the upper panel, we have considered the DHW formalism using a degenerate distribution with $\mu = 4$ and $T = 0.02$, where all the low-energy electron states are filled, preventing further pair creation in the filled region. As shown, due to a strong initial field $E_0 = 4$, pairs are still created at a high rate, but the low-energy region is perfectly blocked. This is seen in Fig. 8 by comparing the momentum distribution $n_D(q)$ after an oscillation period with the initial momentum distribution $n_D(t = 0)$. Specifically, it should be noted that the two curves coincide (no further pair creation) for a low or modest parallel momentum. In the lower panel of Fig. 8, we have used the KGW formalism using the same input data as in the upper panel. We note that pairs are still created for low parallel momentum, in contrast to the DHW case. The effect is expected as the KGW model does not include the effect of the Pauli blocking *dynamically*, even if a degenerate distribution is chosen as an initial condition.

V. CONCLUSION

In this paper, we have compared pair creation in the KGW formalism, based on a Wigner transform of the Klein-Gordon equation, and pair creation in the DHW formalism, based on a Wigner transform of the Dirac equation. First, studying high-frequency pair creation in low amplitude linear theory, we have noted that while the DHW formalism and the KGW formalism share qualitative features (e.g., pair creation when the same resonance condition is fulfilled), the expressions for the wave damping rates due to pair creation are fundamentally different.

Generally, the agreement between KGW and DHW is better for lower frequencies of the electromagnetic field. In particular, if one compensates for the larger magnitude of the vacuum background in the DHW case (by picking a vacuum background a factor 2 larger than for a genuine scalar field), the KGW and DHW equations agree perfectly for the pair-production rate in the zero-frequency limit.

Increasing the frequency of the electric field, the agreement gradually deteriorates. The lack of agreement is correlated with a simultaneous growth of the relative contribution of the polarization current density to the total current density. As the polarization current is a direct consequence of the electron spin, this result is to be expected.

Studying pair production including the back-reaction from the self-consistent current density created by the pairs, the sensitivity to a finite frequency is increased. That is, we need a lower frequency of the electromagnetic field to still get a good agreement between the DHW theory and the KGW theory. Practically speaking $\omega \approx 0.04\omega_c$ or smaller. Moreover, for a self-consistent theory it is crucial to magnify the vacuum background by a factor 2 in the KGW case (as compared to a genuine scalar field), as the nonlinear dynamics otherwise will be heavily modified, in case the self-consistent response has the wrong magnitude. It should also be noted that when the self-consistent field is accounted for, the difference

between KGW and DHW theory tends to increase for very large fields (well above the Schwinger critical field) implying very strong pair creation. This is due to the increase of the self-consistent frequency scale (large number of particles implying a high plasma frequency), and due to the mechanism of Pauli blocking becoming significant in the DHW theory

Moreover, we have isolated the mechanism of Pauli blocking by studying the case of degenerate initial distributions. As expected, in the DHW formalism pairs can not be created in a region of momentum space where the states are occupied. The same does not apply for the KGW formalism, naturally.

In this paper, we have compared numerical results from the KGW formalism specifically with the DHW formalism. However, it can be noted that there are other well-established approaches to the problem of strong field pair creation, e.g., the quantum kinetic formalism [7,41–43] related to the quantum mechanical scattering approach and S-matrix theory [44,45]. Importantly, in the homogeneous and vanishing magnetic field limit (the geometry studied in the numerical section of this paper), it has been shown that the DHW formalism agrees exactly with the quantum kinetic theory [7,41–43]. Thus, in practice, much of the present comparison of the KGW formalism with the DHW theory is also a comparison with quantum kinetic theory.

The present paper is motivated by a desire to use the KGW formalism whenever it is a valid approximation, as the 16 scalar equations of the DHW formalism (as compared to the four scalar equations of the KGW formalism) are considerably more difficult to solve, both numerically and analytically. While the present paper has certain restrictions, e.g., except for Sec. III we have considered electrostatic fields and the ho-

mogeneous limit, we expect that many of the present findings apply in more general scenarios.

To give some motivation for this belief, let us consider a more general scenario, where the field has a magnetic component, and is varying both temporarily and spatially. First, we note that strong field pair creation is driven by the electromagnetic invariant $E^2 - B^2$. If this quantity is positive (such that strong field pair creation is possible), there exists a reference frame where the field is purely electric. Analyzing the local (ignoring temporal and spatial gradients) physics in the reference frame of a pure electric field, we will obtain agreement between DHW and KGW theory, as locally we can view the field as electric as well as homogeneous. More realistically, however, the agreement will fail, to the extent that the local approximation is not accurate enough. However, from a relativistic point of view, whether the deviation from locality is temporal or spatial is again dependent on the reference frame. Specifically, for a field that can be locally approximated by a plane wave, only the invariant $\omega^2 - k^2$ matters. If this quantity is positive, there exists a frame where the variation is purely temporal, in which case the findings of the present paper, with a maximum allowed frequency for the KGW theory, would be applicable.

Thus, we expect that the relatively good agreement between the DHW formalism and the KGW formalism for low frequencies generalizes to cases of spatial variations and electromagnetic fields, at least qualitatively. However, more studies are needed to give a definitive answer.

[1] C. N. Danson, C. Haefner, J. Bromage, T. Butcher, J.-C. F. Chanteloup, E. A. Chowdhury, A. Galvanauskas, L. A. Gizzi, J. Hein, D. I. Hillier *et al.*, Petawatt and exawatt class lasers worldwide, High Power Laser Sci. Eng. **7**, e54 (2019).

[2] E. Cartlidge, The light fantastic, Science **359**, 382 (2018).

[3] A. Di Piazza, C. Müller, K. Z. Hatsagortsyan, and C. H. Keitel, Extremely high-intensity laser interactions with fundamental quantum systems, Rev. Mod. Phys. **84**, 1177 (2012).

[4] A. Fedotov, A. Ilderton, F. Karbstein, B. King, D. Seipt, H. Taya, and G. Torgrimsson, Advances in QED with intense background fields, Phys. Rep. **1010**, 1 (2023).

[5] F. Sauter, Über das verhalten eines elektrons im homogenen elektrischen feld nach der relativistischen theorie diracs, Z. Angew. Phys. **69**, 742 (1931).

[6] J. Schwinger, On gauge invariance and vacuum polarization, Phys. Rev. **82**, 664 (1951).

[7] F. Hebenstreit, R. Alkofer, and H. Gies, Schwinger pair production in space- and time-dependent electric fields: Relating the wigner formalism to quantum kinetic theory, Phys. Rev. D **82**, 105026 (2010).

[8] F. Hebenstreit, R. Alkofer, and H. Gies, Particle self-bunching in the schwinger effect in spacetime-dependent electric fields, Phys. Rev. Lett. **107**, 180403 (2011).

[9] I. A. Aleksandrov and C. Kohlfürst, Pair production in temporally and spatially oscillating fields, Phys. Rev. D **101**, 096009 (2020).

[10] C. Kohlfürst, Effect of time-dependent inhomogeneous magnetic fields on the particle momentum spectrum in electron-positron pair production, Phys. Rev. D **101**, 096003 (2020).

[11] S. S. Bulanov, V. D. Mur, N. B. Narozhny, J. Nees, and V. S. Popov, Multiple colliding electromagnetic pulses: A way to lower the threshold of e^+e^- pair production from vacuum, Phys. Rev. Lett. **104**, 220404 (2010).

[12] A. Gonoskov, I. Gonoskov, C. Harvey, A. Ilderton, A. Kim, M. Marklund, G. Mourou, and A. Sergeev, Probing nonperturbative qed with optimally focused laser pulses, Phys. Rev. Lett. **111**, 060404 (2013).

[13] G. Torgrimsson, C. Schneider, and R. Schützhold, Sauter-schwinger pair creation dynamically assisted by a plane wave, Phys. Rev. D **97**, 096004 (2018).

[14] C. Kohlfürst, N. Ahmadiniaz, J. Oertel, and R. Schützhold, Sauter-schwinger effect for colliding laser pulses, Phys. Rev. Lett. **129**, 241801 (2022).

[15] N. B. Narozhnyi and A. I. Nikishov, Pair production by an electric field, Zh. Eksp. Teor. Fiz **65**, 862 (1974) [Sov. Phys. JETP **38**, 427 (1974)].

[16] C. Kohlfürst, Spin states in multiphoton pair production for circularly polarized light, Phys. Rev. D **99**, 096017 (2019).

[17] C. Kohlfürst, The Heisenberg-Wigner formalism for transverse fields, arXiv:2212.06057.

[18] J. C. R. Bloch, V. A. Mizerny, A. V. Prozorkevich, C. D. Roberts, S. M. Schmidt, S. A. Smolyansky, and D. V. Vinnik, Pair creation: Back reactions and damping, Phys. Rev. D **60**, 116011 (1999).

[19] F. Cooper and E. Mottola, Quantum back reaction in scalar qed as an initial-value problem, Phys. Rev. D **40**, 456 (1989).

[20] Y. Kluger, J. M. Eisenberg, B. Svetitsky, F. Cooper, and E. Mottola, Pair production in a strong electric field, Phys. Rev. Lett. **67**, 2427 (1991).

[21] S. P. Kim and D. N. Page, Schwinger pair production in electric and magnetic fields, Phys. Rev. D **73**, 065020 (2006).

[22] Y. Shi, J. Xiao, H. Qin, and N. J. Fisch, Simulations of relativistic quantum plasmas using real-time lattice scalar qed, Phys. Rev. E **97**, 053206 (2018).

[23] I. Bialynicki-Birula, P. Gornicki, and J. Rafelski, Phase-space structure of the Dirac vacuum, Phys. Rev. D **44**, 1825 (1991).

[24] C. Best, P. Gornicki, and W. Greiner, The phase-space structure of the Klein-Gordon field, Ann. Phys. (NY) **225**, 169 (1993).

[25] K. Li, J. Wang, S. Dulat, and K. Ma, Wigner functions for klein-gordon oscillators in non-commutative space, Int. J. Theor. Phys. **49**, 134 (2010).

[26] J. Santos and L. Silva, Wigner-Moyal description of free variable mass Klein-Gordon fields, J. Math. Phys. **46**, 102901 (2005).

[27] C.-Y. Wong, Klein-Gordon equation in hydrodynamical form, J. Math. Phys. **51**, 122304 (2010).

[28] P. Zhuang and U. Heinz, Equal-time hierarchies for quantum transport theory, Phys. Rev. D **57**, 6525 (1998).

[29] Z. L. Li, B. S. Xie, and Y. J. Li, Boson pair production in arbitrarily polarized electric fields, Phys. Rev. D **100**, 076018 (2019).

[30] A. Nikishov, Pair production by a constant external field, Sov. Phys. JETP **30**, 660 (1970).

[31] H. Feshbach and F. Villars, Elementary relativistic wave mechanics of spin 0 and spin 1/2 particles, Rev. Mod. Phys. **30**, 24 (1958).

[32] H. Al-Naseri, J. Zamanian, and G. Brodin, Plasma dynamics and vacuum pair creation using the Dirac-Heisenberg-Wigner formalism, Phys. Rev. E **104**, 015207 (2021).

[33] G. Brodin and J. Zamanian, Quantum kinetic theory of plasmas, Rev. Mod. Plasma Phys. **6**, 4 (2022).

[34] H. Al-Naseri and G. Brodin, Linear pair-creation damping of high-frequency plasma oscillation, Phys. Plasmas **29**, 042106 (2022).

[35] G. Brodin, H. Al-Naseri, J. Zamanian, G. Torgrimsson, and B. Eliasson, Plasma dynamics at the schwinger limit and beyond, Phys. Rev. E **107**, 035204 (2023).

[36] W. H. Press, S. A. Teukolsky, W. T. Vetterling, and B. P. Flannery, *Numerical Recipes: The Art of Scientific Computing*, 3rd ed. (Cambridge University Press, New York, 2007).

[37] M. Stefan, J. Zamanian, G. Brodin, A. P. Misra, and M. Marklund, Ponderomotive force due to the intrinsic spin in extended fluid and kinetic models, Phys. Rev. E **83**, 036410 (2011).

[38] F. A. Asenjo, J. Zamanian, M. Marklund, G. Brodin, and P. Johansson, Semi-relativistic effects in spin-1/2 quantum plasmas, New J. Phys. **14**, 073042 (2012).

[39] We note that the difference between q and p_z is not important for high frequency pair creation as this process will take place also for small/modest electric field, which leads to a small A.

[40] K. Krajewska and J. Z. Kamiński, Threshold effects in electron-positron pair creation from the vacuum: Stabilization and longitudinal versus transverse momentum sharing, Phys. Rev. A **100**, 012104 (2019).

[41] S. Smolyansky, G. Röpke, S. Schmidt, D. Blaschke, V. Toneev, and A. Prozorkevich, Dynamical derivation of a quantum kinetic equation for particle production in the Schwinger mechanism, arXiv:hep-ph/9712377.

[42] S. Schmidt, D. Blaschke, G. Röpke, S. Smolyansky, A. Prozorkevich, and V. Toneev, A quantum kinetic equation for particle production in the Schwinger mechanism, Int. J. Mod. Phys. E **07**, 709 (1998).

[43] Y. Kluger, E. Mottola, and J. M. Eisenberg, Quantum vlasov equation and its Markov limit, Phys. Rev. D **58**, 125015 (1998).

[44] C. K. Dumlu, Quantum kinetic approach and the scattering approach to vacuum pair production, Phys. Rev. D **79**, 065027 (2009).

[45] A. M. Fedotov, E. G. Gelfer, K. Y. Korolev, and S. A. Smolyansky, Kinetic equation approach to pair production by a time-dependent electric field, Phys. Rev. D **83**, 025011 (2011).